

## PAPER

## An isotropic sound field model composed of a finite number of plane waves

Tatsuhiko Tanaka\* and Makoto Otani

*Graduate School of Engineering, Kyoto University,  
Kyoto daigaku-Katsura, Nishikyo-ku, Kyoto, 615–8540 Japan**(Received 2 September 2022, Accepted for publication 27 February 2023)*

**Abstract:** Isotropy is a fundamental property of a diffuse sound field. Although several studies have proposed an isotropy indicator to quantify the extent of the isotropy of a sound field, what is not yet very clear is how to interpret the quantified isotropy using these indicators. This study aims to contribute to the understanding of the isotropy by (i) modifying an existing isotropy indicator based on the spherical harmonic expansion and (ii) presenting isotropic sound field model composed of a finite number of plane waves. Theoretical and numerical investigations show that a limited-degree isotropy can be established by using the isotropy indicator and the isotropic sound field model.

**Keywords:** Isotropy, Rotational invariance, Isotropic sound field, Spherical design

## 1. INTRODUCTION

Successful modeling of the directional energy distribution (DED) of sound fields should help refine sound absorption coefficient measurements in a reverberation room [1] and realize efficient psychophysical experiments to clarify the mechanism of spatial auditory perception such as the auditory source width or the listener envelopment [2–5]. Here, the DED refers to the distributions of the energy from each direction observed at a certain point in a room, where the sound field is composed of plane waves.

To model an arbitrary DED, a method must be constructed that can appropriately simulate DEDs for two extremes: the most non-uniform and the most uniform cases. A sound field with the most non-uniform DED is one in which a single plane wave arrives from only one direction. In contrast, it is debatable how to define a sound field with the most uniform DED.

Based on the concept of a diffuse sound field originating from Sabine [6, Chap. 1], the physical properties of a diffuse sound field are roughly divided into two parts:

**Homogeneity** Uniform distribution of the acoustic energy in a room.

**Isotropy** Statistical uniformity of the directional properties (e.g., the arrival direction of a sound wave) in the sound field observed at a point in a room.

This paper focuses on the isotropy. As in previous studies [7], the term “isotropy” is used to express the uniformity of DED in this paper.

Here, the plane-wave model (PWM, see Ref. [8, Sect. II.B] for example) is regarded as a theoretical model of the isotropic sound field. In PWM, the sound field is composed of an infinite number of plane waves arriving from all directions. Random variables determine the amplitude and phase of each plane wave. Although PWM is essentially a theoretical model for a diffuse sound field, it is reasonable to treat PWM as a theoretical model of the isotropic sound field since the diffuseness encompasses the isotropy.

Among the isotropy indicators proposed to date, most evaluate the isotropy of a sound field using the following physical quantities:

- Deviation of the energy decay curves calculated for select directions [9–12];
- Ratio of the zeroth-degree spherical harmonic expansion coefficients (SHEC) of the temporarily integrated DED [7,13–15].

These indicators quantify an isotropy by evaluating the uniformity of the directional distribution of physical quantities such as energy decay curves or the temporarily integrated absolute amplitudes of plane waves [13]. Indicators [9–12] using the variance or deviation of energy decay curves for each direction depend on the set of directions selected in the calculation. Therefore, the set of directions must be carefully selected to calculate these indicators. In contrast, the isotropy indicators [7,13–15] using SHECs of a DED do not explicitly require such a selection and are more concise. Hence, the current study focuses on them.

Since the perfectly isotropic sound field is generated by the superposition of an infinite number of plane waves, infinitely precise directional resolution is required to

\*e-mail: tanaka.tatsuhiko@icloud.com  
[doi:10.1250/ast.44.317]

evaluate the isotropy of a sound field. However, existing isotropy indicators quantify an isotropy of sound fields employing microphone arrays with a finite number of microphones or finitely precise directional resolution. Thus, it remains unclear how to understand the quantified isotropy using the existing indicators. The assumption of an infinite number of plane waves in PWM is considered to be the cause of these problems. Therefore, it is necessary to construct an isotropic sound field model that assumes a finite number of plane waves and finitely precise directional resolution.

To develop an understanding of the isotropy, this paper (i) enhances the usefulness of the existing isotropy indicators by modifying them from a viewpoint of rotational invariance, and (ii) proposes an isotropic sound field model composed of a finite number of plane waves using spherical designs.

The rest of this paper is organized as follows. Section 2 defines the cumulative DED. Section 3 numerically illustrates rotationally variant/invariant nature of the isotropy indicators, later, in Sect. 6, more practical numerical/experimental examinations of them are given. Section 4 formulates a limited-degree isotropic sound field model based on the spherical design. The model is then numerically constructed in Sect. 5.

## 2. CUMULATIVE DIRECTIONAL ENERGY DISTRIBUTION

### 2.1. Sound Field Composed of Plane Waves

Here, a sound field composed of sinusoidal plane waves is considered. The sound field is written as

$$P(\mathbf{r}, k, \tau) = \sum_{q=1}^Q A_q(k, \tau) \cdot e^{i\mathbf{k}n_q \cdot \mathbf{r}}, \quad i := \sqrt{-1}, \quad (1)$$

where  $\mathbf{r} = (x, y, z)$  is an observation point;  $\mathbf{n}_q$  is a unit vector pointing at direction of arrival (DoA) of  $q$ th plane wave;  $A_q(k, \tau)$  is the complex amplitude of  $q$ th plane wave at the origin in the domain of short-time Fourier transform.  $\tau$  [s] is the center of the time window.  $k$  [rad/m] is the wavenumber of the plane waves.

### 2.2. Cumulative Directional Energy Distribution

Since the isotropy of a sound field is a statistical or cumulative property, it is more reasonable to estimate the isotropy using cumulative DEDs than instantaneous ones. The cumulative or Schroeder-integrated DED in the spherical-harmonics domain and the SHECs of that are given respectively as

$$\hat{D}_N^c(\theta, \phi; k, \tau) := \sum_{n=0}^N \sum_{m=-n}^n \hat{a}_{n,m}^c(k, \tau) \cdot Y_{n,m}^c(\theta, \phi), \quad (2)$$

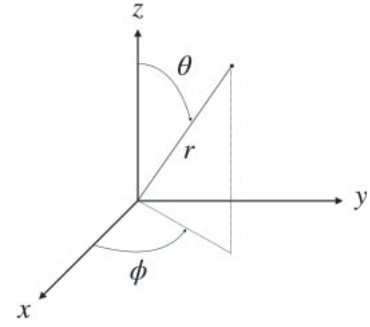


Fig. 1 Spherical coordinate system.

$$\hat{a}_{n,m}^c(k, \tau) := \sum_{q=1}^Q \left( \frac{1}{T - \tau} \int_{\tau}^T |A_q(k, \tau')|^2 d\tau' \right) \times \overline{Y_{n,m}^c(\theta_q, \phi_q)}, \quad (3)$$

where  $Y_{n,m}^c$  is the complex-valued spherical harmonics (A.1) and  $n = 0, 1, \dots, N$  and  $m = 0, \pm 1, \dots, \pm n$  are the degree and order, respectively.  $\overline{(\cdot)}$  represents the complex conjugate.  $0 \leq \theta_q \leq \pi$  and  $-\pi \leq \phi_q < \pi$  are the angular coordinates in the spherical coordinate system (Fig. 1). These represent the DoA of  $q$ th plane wave. Hereafter, the case of  $\tau = 0$  and  $T = \infty$  is considered, unless otherwise noted. Thus, the cumulative DED and the SHECs of that are rewritten respectively as

$$D_N^c(\theta, \phi; k) := \sum_{n=0}^N \sum_{m=-n}^n a_{n,m}^c(k) \cdot Y_{n,m}^c(\theta, \phi), \quad (4)$$

$$a_{n,m}^c(k) := \sum_{q=1}^Q \left( \lim_{T \rightarrow \infty} \frac{1}{T} \int_0^T |A_q(k, \tau)|^2 d\tau \right) \times \overline{Y_{n,m}^c(\theta_q, \phi_q)} \quad (5)$$

$$= \sum_{q=1}^Q E[|A_q(k, \tau)|^2] \cdot \overline{Y_{n,m}^c(\theta_q, \phi_q)},$$

where  $E[\cdot]$  denotes the expected value or time average.

## 3. ISOTROPY INDICATORS

This section introduces the existing isotropy indicators to evaluate the isotropy of the DED in a sound field. Simple numerical experiments show the rotationally variant nature of the 1-norm isotropy indicator [7] and the rotationally invariant nature of the 2-norm isotropy indicator, which is given by modifying the existing isotropy indicator [14].

### 3.1. 1-norm Isotropy Indicator

Nolan *et al.* [7] proposed an isotropy indicator in 2018. This indicator is defined as the ratio of the absolute value of the zeroth-degree spherical harmonic expansion coefficient (SHEC) of a sound field to the sum of the absolute value of SHECs of that from zeroth to  $N$ th degree, which is given as

$$v_N^c(k) := \frac{\|\mathbf{a}_0^c(k)\|_1}{\sum_{n=0}^N \|\mathbf{a}_n^c(k)\|_1}, \quad (6)$$

where

$$\|\mathbf{a}_n^c(k)\|_1 := \sum_{m=-n}^n |a_{n,m}^c(k)|. \quad (7)$$

The indicator given above is henceforth referred to as the 1-norm isotropy indicator in this paper. By applying the indicator (6) to the SHECs (5) of the cumulative DED, the statistical isotropy of the sound field can be evaluated. Here, its rotationally variant nature is considered.

Below, a simple example is numerically demonstrated to show the rotationally variant problem. A sound field consisting of a single plane wave arriving from a fixed direction is considered. For simplicity, the time-averaged energy of the plane wave is set to 1:

$$\lim_{T \rightarrow \infty} \frac{1}{T} \int_0^T |A_{\text{sgl}}(k, \tau)|^2 d\tau = 1. \quad (8)$$

SHECs of the cumulative DED of this sound field are given as

$$a_{n,m}^{\text{c,sgl}} = \overline{Y_{n,m}^{\text{C}}(\theta_{\text{in}}, \phi_{\text{in}})}, \quad (9)$$

where  $(\theta_{\text{in}}, \phi_{\text{in}})$  is the DoA of the single plane wave.

In this case, it is reasonable to consider the isotropy of the cumulative DED as a constant regardless of the DoA of the plane wave. Supposing that the 1-norm isotropy indicator (6) is applied to the cumulative DED, it may thus be desirable that its numerical value

$$v_N^{\text{c,sgl}} := \frac{\|\mathbf{a}_0^{\text{c,sgl}}\|_1}{\sum_{n=0}^N \|\mathbf{a}_n^{\text{c,sgl}}\|_1} \quad (10)$$

should be constant regardless of the DoA  $(\theta_{\text{in}}, \phi_{\text{in}})$  of the plane wave.

Figure 2 shows the numerical values of the 1-norm isotropy indicator (10) applied to the cumulative DED for select DoAs  $(\theta_{\text{in}}, \phi_{\text{in}})$  and truncation degrees  $N$ . The value of the 1-norm indicator is not constant with variations in the DoA of the plane wave, implying that the 1-norm isotropy indicator is not rotationally invariant.

In order to demonstrate another problem caused by the rotationally variant nature of the 1-norm isotropy indicator, Sect. 6.1 shows the results of applying the 1-norm indicator to the limited-degree isotropic models, which is to be presented later.

### 3.2. 2-norm Isotropy Indicator

To cope with the rotationally variant issue of the 1-norm isotropy indicator (6), an isotropy indicator based on the 2-norm of SHECs is considered.

Here, the 2-norm isotropy indicator is formulated as follows.

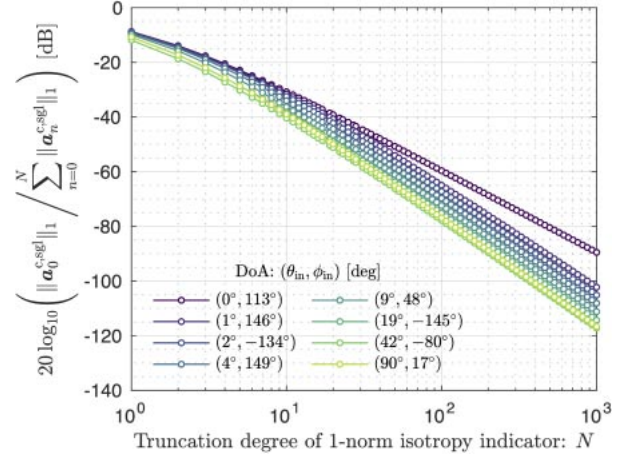


**Fig. 2** Numerical values of the 1-norm isotropy indicator (10) applied to the SHECs (9) for a sound field consisting of a single plane wave. For the DoA of the plane wave,  $\theta_{\text{in}}$  increases logarithmically from  $0^\circ$  to  $90^\circ$ , while  $\phi_{\text{in}}$  varies randomly from  $-180^\circ$  to  $180^\circ$ , respectively. Truncation degree  $N$  increases logarithmically from 1 to 1,000. These conditions also apply to Fig. 3.

$$\mu_N^c(k) := \frac{\|\mathbf{a}_0^c(k)\|_2}{\sum_{n=0}^N \|\mathbf{a}_n^c(k)\|_2}, \quad (11)$$

where  $\|\mathbf{a}_n^c(k)\|_2$  is given as

$$\|\mathbf{a}_n^c(k)\|_2 := \left( \sum_{m=-n}^n |a_{n,m}^c(k)|^2 \right)^{1/2}. \quad (12)$$

The 2-norm isotropy indicator (11) is essentially the same as the one proposed by Ebeling [14] (and rediscovered by Nolan *et al.* [15] in 2016), but this study makes a minor modification to be consistent with the 1-norm isotropy indicator (6).

Since the square sum of  $n$ th-degree SHECs has been proven to be rotationally invariant [16, Prop. 2.1], its root (12) and the 2-norm isotropy indicator (11) are also rotationally invariant.

The 2-norm isotropy indicator can also be applied to SHECs (9) for a sound field consisting of a single plane wave

$$\mu_N^{\text{c,sgl}} := \frac{\|\mathbf{a}_0^{\text{c,sgl}}\|_2}{\sum_{n=0}^N \|\mathbf{a}_n^{\text{c,sgl}}\|_2}. \quad (13)$$

Figure 3 depicts the results of the numerical experiment. Unlike the results for the 1-norm isotropy indicator (Fig. 2), the numerical value of the 2-norm isotropy indicator (13) is constant regardless of the DoA  $(\theta_{\text{in}}, \phi_{\text{in}})$  of the plane wave. These results suggest that the 2-norm isotropy indicator (11) has a rotationally invariant property, and is favorable for evaluating isotropy. Therefore, this study employs the 2-norm isotropy indicator to evaluate the isotropy.

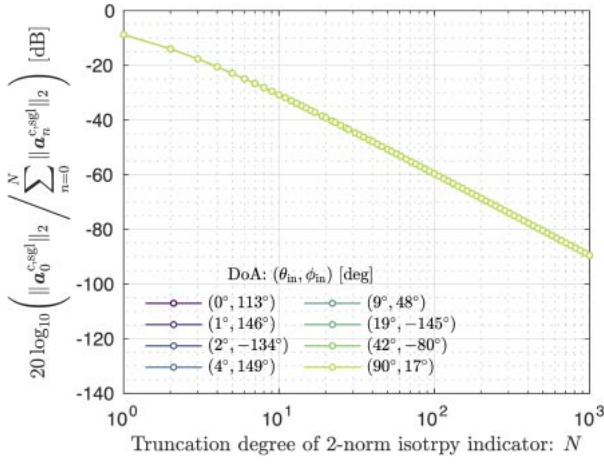


Fig. 3 Numerical values of the 2-norm isotropy indicator (13) applied to SHECs (9) for the sound field consisting of a single plane wave.

In Sect. 6.2, the 2-norm isotropy indicator is applied to some RIRs [17] in order to demonstrate the usefulness and limitations of the indicator.

### 3.3. Truncation Degree of the Isotropy Indicators

Figures 2 and 3 illustrate not only the dependence/independence of the numerical values of the isotropy indicators on the DoA of the plane wave but also the numerical behavior of the indicators with the variations of the truncation degree  $N$  (defined in Eqs. (6) and (11), respectively). The numerical values of both indicators decrease exponentially in an inverse proportion to the truncation degree.

It may be problematic that the numerical values of the indicators for the same sound field vary with the truncation degree. Nevertheless, this is likely to be unavoidable, regardless of which of the existing isotropy indicators is adopted. In fact, the numerical values of all the isotropy indicators mentioned in Sect. 1 depend on the directional resolution. Therefore, this study makes use of the truncation-degree dependence of the 2-norm isotropy indicator in the concept of a limited-degree isotropy proposed in Sect. 4.

## 4. LIMITED-DEGREE ISOTROPIC SOUND FIELD MODEL

This section presents a concept called limited-degree isotropy, which represents the isotropy for a given limitation on the directional resolution. By introducing the limited-degree isotropy, a spherical design can be used to model an isotropic sound field consisting of a finite number of plane waves.

### 4.1. Sound Field in PWM

In PWM [8, Sect. II.B], the complex amplitude at a

certain time for each plane wave that composes the (diffuse) sound field is given as [18,19]

$$A_q^{pwm}(k, \tau) = \frac{\alpha_q(k, \tau) + i\beta_q(k, \tau)}{\sqrt{Q}}, \quad (14)$$

where  $\alpha_q$  and  $\beta_q$  are independent zero-mean Gaussian random variables whose variance is  $1/2$ .  $Q$  is the total number of plane waves that compose the sound field. Since  $Q$  is infinite in theory, the SHECs of the cumulative DED of this sound field are given as

$$\begin{aligned} a_{n,m}^{pwm}(k) &= \lim_{Q \rightarrow \infty} \sum_{q=1}^Q \left( \lim_{T \rightarrow \infty} \frac{1}{T} \int_0^T |A_q^{pwm}(k, \tau)|^2 d\tau \right) \\ &\quad \times \overline{Y_{n,m}^C(\theta_q, \phi_q)} \\ &= \lim_{Q \rightarrow \infty} \sum_{q=1}^Q E[|A_q^{pwm}(k, \tau)|^2] \cdot \overline{Y_{n,m}^C(\theta_q, \phi_q)} \\ &= \lim_{Q \rightarrow \infty} \sum_{q=1}^Q \frac{E[\{\alpha_q(k, \tau)\}^2 + \{\beta_q(k, \tau)\}^2]}{Q} \\ &\quad \times \overline{Y_{n,m}^C(\theta_q, \phi_q)} \\ &= \lim_{Q \rightarrow \infty} \sum_{q=1}^Q (1/Q) \overline{Y_{n,m}^C(\theta_q, \phi_q)} \\ &\stackrel{?}{=} \begin{cases} (4\pi)^{-1/2}, & n = 0. \\ 0, & n = 1, 2, \dots \end{cases} \end{aligned} \quad (15)$$

The last transformation of the equation is based on the assumption that the plane waves arrive from all directions.

Although the above result is easily predictable based on the previous studies discussing the perfect isotropy, it suggests that PWM (infinite number of plane waves) can synthesize the perfectly isotropic sound field in the spherical-harmonics domain.

However, the infinite number of plane waves assumed in PWM gives little suggestions as to a method of quantifying the extent of the isotropy of a sound field and an interpretation of an isotropy quantified in some way. To solve this problem, a spherical design is introduced as the DoAs of the plane waves.

### 4.2. Spherical Design

**Definition 1** (Delsarte *et al.* [20, Def. 5.1]). For any polynomial function  $p_{\leq t}(\theta, \phi)$  of degree  $t$  at most defined on the unit sphere  $\mathbb{S}^2$  in three-dimensional Euclidean space, the point set  $\hat{\Phi}_Q = \{(\hat{\theta}_q, \hat{\phi}_q); q = 1, 2, \dots, Q\}$  satisfying the following equality is the spherical  $t$ -design on  $\mathbb{S}^2$

$$\frac{1}{Q} \sum_{q=1}^Q p_{\leq t}(\hat{\theta}_q, \hat{\phi}_q) = \frac{1}{4\pi} \int_{-\pi}^{\pi} \int_0^{\pi} p_{\leq t}(\theta, \phi) \sin \theta d\theta d\phi. \quad (16)$$

Equation (16) implies that the integral of any polynomial function  $p_{\leq t}(\theta, \phi)$  on  $\mathbb{S}^2$  can be computed exactly

if given an upper bound on the degree by summing the discretely sampled function values on the spherical  $t$ -design  $\Phi_Q$ . (In this study, the term ‘‘spherical  $t$ -design’’ is sometimes used to emphasize the degree of the spherical design.)

An equivalence transformation of definition 1 yields the following theorem using real-valued spherical harmonics (A.2)

**Theorem 1** (Womersley [21, Sect. 4.1]). A point set  $\Phi_Q = \{(\hat{\theta}_q, \hat{\phi}_q); q = 1, 2, \dots, Q\}$  is the spherical  $t$ -design on  $\mathbb{S}^2$  if and only if the following equation holds for  $\Phi_Q$

$$\sum_{q=1}^Q Y_{n,m}^{\mathbb{R}}(\hat{\theta}_q, \hat{\phi}_q) = 0 \quad (17)$$

for  $n = 1, 2, \dots, t$  and  $m = 0, \pm 1, \dots, \pm n$ .

**Proposition 1.** If and only if Eq. (17) holds for  $n = 1, 2, \dots, t$  and  $m = 0, \pm 1, \dots, \pm n$ , then the following equation using complex-valued spherical harmonics also holds

$$\sum_{q=1}^Q Y_{n,m}^{\mathbb{C}}(\hat{\theta}_q, \hat{\phi}_q) = 0 \quad (18)$$

for  $n = 1, 2, \dots, t$  and  $m = 0, \pm 1, \dots, \pm n$ .

The above Proposition is proven in Appendix B.

### 4.3. Modeling an Isotropic Sound Field by Using Spherical Design

Consider the case where each plane wave has a complex amplitude, which is given in Eq. (14), and the DoAs  $\{(\hat{\theta}_q, \hat{\phi}_q); q = 1, 2, \dots, Q\}$  of the plane waves are sampled on the spherical design. The SHECs of the cumulative DED of the sound field synthesized by superimposing these plane waves are given as

$$\begin{aligned} a_{n,m}^{\mathbb{C},t}(k) &= \sum_{q=1}^Q \left( \lim_{T \rightarrow \infty} \frac{1}{T} \int_0^T |A_q^{\text{PwM}}(k, \tau)|^2 d\tau \right) \\ &\quad \times \overline{Y_{n,m}^{\mathbb{C}}(\hat{\theta}_q, \hat{\phi}_q)} \\ &\stackrel{(15)}{=} (1/Q) \sum_{q=1}^Q \overline{Y_{n,m}^{\mathbb{C}}(\hat{\theta}_q, \hat{\phi}_q)} \\ &\stackrel{(18)}{=} \begin{cases} (4\pi)^{-1/2}, & n = 0. \\ 0, & n = 1, 2, \dots, t. \end{cases} \end{aligned} \quad (19)$$

By applying the 2-norm isotropy indicator to the SHECs (19), the following equality holds for the truncation degrees such that  $N \leq t$

$$\mu_{N \leq t}^{\mathbb{C},t}(k) = \frac{\|\mathbf{a}_0^{\mathbb{C},t}\|_2}{\sum_{n=0}^N \|\mathbf{a}_n^{\mathbb{C},t}\|_2} = \frac{\|\mathbf{a}_0^{\mathbb{C},t}\|_2}{\|\mathbf{a}_0^{\mathbb{C},t}\|_2} = \frac{(4\pi)^{-1/2}}{(4\pi)^{-1/2}} = 1. \quad (20)$$

The above results suggest that a finite number of plane waves can synthesize a perfectly isotropic sound field for a given upper bound of the degree. In addition, the present results suggest the concept of the isotropy with an upper

bound of the degree, which is the main contribution of this paper.

The concept is hereinafter referred to as *the limited-degree isotropy*. (Equation (20) represents ‘‘ $t$ th-degree isotropy.’’) Among the sound fields with  $t$ th-degree isotropy, those with  $Q = (t + 1)^2$  plane waves are called the ‘‘ $t$ th-degree isotropic sound field model’’ in this study. (However, it is possible to construct a spherical  $t$ -design for a smaller number of points. For example, Womersley [21] successfully constructed (numerical) spherical designs with approximately  $(t + 1)^2/2$  points.)

### 4.4. Summary and Limitations of Limited-degree Isotropic Sound Field Model

The proposed limited-degree isotropic sound field model consists of  $(t + 1)^2$  plane waves arriving from directions sampled with a spherical  $t$ -design. The complex amplitude of each plane wave at a given time is determined by independent standard normal complex random variables. The cumulative DED in the model satisfies the  $t$ th-degree isotropy.

A note of caution is due here since the infinite time integral is assumed in the process of constructing the model. The assumption limits the application of the model to a simulated or measured sound field. Thus, the effectiveness of the model in the practical situations remains to be studied.

## 5. NUMERICAL MODELLING OF LIMITED-DEGREE ISOTROPIC SOUND FIELD

### 5.1. Approximation of Spherical Design

This subsection describes how to construct an approximate (or numerical) spherical design using the nonlinear least-squares method, which is briefly presented in Ref. [21, Sect. 4.4]. First, the following vector-valued function is given as

$$\begin{aligned} \mathbf{r}_t^{\mathbb{R}}(\Phi_Q) &:= \left[ \sum_{q=1}^Q Y_{1,-1}^{\mathbb{R}}(\theta_q, \phi_q), \sum_{q=1}^Q Y_{1,0}^{\mathbb{R}}(\theta_q, \phi_q), \right. \\ &\quad \left. \sum_{q=1}^Q Y_{1,1}^{\mathbb{R}}(\theta_q, \phi_q), \dots, \sum_{q=1}^Q Y_{t,t}^{\mathbb{R}}(\theta_q, \phi_q) \right]^{\top}. \end{aligned} \quad (21)$$

From Theorem 1, the point set  $\Phi_Q^*$  that satisfies equation  $\mathbf{r}_t^{\mathbb{R}}(\Phi_Q^*) = \mathbf{0}$  is a spherical design. Instead of solving the equation  $\mathbf{r}_t^{\mathbb{R}}(\Phi_Q) = \mathbf{0}$ , the sum of the squares of the elements of the original vector-valued function (21) is minimized by the nonlinear least-squares method. Namely, the following objective function is minimized.

$$f_t^{\mathbb{R}}(\Phi_Q) := \mathbf{r}_t^{\mathbb{R}}(\Phi_Q)^{\top} \mathbf{r}_t^{\mathbb{R}}(\Phi_Q). \quad (22)$$

Note that point set  $\Phi_Q^*$  that satisfies  $f_t^{\mathbb{R}}(\Phi_Q^*) = 0$  is also a spherical design.

The Levenberg-Marquardt method (L-M method [22,23]) is employed to obtain an approximate spherical  $t$ -design with  $(t+1)^2$  points (i.e., a local minimum solution of objective function (22)). The L-M method is a hybrid of the steepest descent and Gauss-Newton methods. It has advantages of both. That is, the L-M method reduces the function value at each iteration and has a fast convergence around the solution.

The iterations are stopped once one of the following conditions is achieved

$$\|\nabla f_t^{\text{IR}}(\Phi_{Q,t+1})\|_{\infty} < 10^{-13}, \quad (23)$$

$$\frac{\|\Phi_{Q,t+1} - \Phi_{Q,t}\|_{\infty}}{\|\Phi_{Q,t}\|_{\infty}} < 10^{-10}, \quad (24)$$

where  $\Phi_{Q,l}$  is the approximate solution obtained at the  $l$ th iteration.  $\|\mathbf{x}\|_{\infty}$  equals to the maximum absolute value of the elements of vector  $\mathbf{x}$ .

The initial approximate solution is set to the maximum determinant (MaxDet [24]), while the initial value of the trust parameter for the L-M method is  $\lambda_0 = 10^{-2}$ . The calculations are performed using the MATLAB [25] command `lsqnonlin`. (In `lsqnonlin`, conditions (23) and (24) correspond with `FunctionTolerance = 1e-9` and `StepTolerance = 1e-10`, respectively.)

## 5.2. Isotropy of Limited-degree Isotropic Sound Field Model Using Approximate Spherical Design

The isotropy of the approximate limited-degree isotropic model is evaluated. The accuracy of the isotropy realized by the approximate limited-degree model is assessed using the following measure

$$\Pi_t[n] := \frac{\|\mathbf{a}_n^{c,t}\|_2}{\sum_{j=0}^t \|\mathbf{a}_j^{c,t}\|_2}, \quad n = 0, 1, \dots, t, \quad (25)$$

where,  $t$  is the degree of an isotropic model. If an isotropic

sound field is generated by a strict spherical design (18), the following equality is realized

$$\Pi_t[n] = \begin{cases} 1, & n = 0. \\ 0, & n = 1, 2, \dots, t. \end{cases} \quad (26)$$

Equation (26) enables the accuracy of the isotropy of the approximate isotropic model to be evaluated by the smallness of the numerical value of  $\Pi_t[n]$  for  $n = 1, 2, \dots, t$ .

Figure 4 shows the calculation results of measure (25) using the SHECs

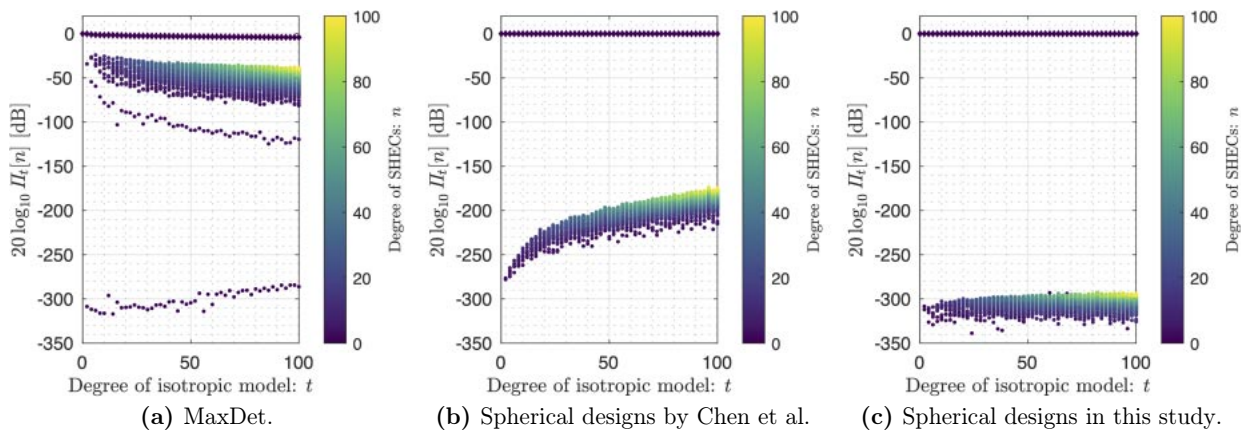
$$\mathbf{a}_{n,m}^{c,t} = (1/Q) \sum_{q=1}^Q Y_{n,m}^C(\hat{\theta}_q, \hat{\phi}_q) \quad (27)$$

for sample DoAs  $(\hat{\theta}_q, \hat{\phi}_q)$ : MaxDet [24], spherical designs by Chen *et al.* [26], and the spherical designs computed in this study. Compared with the other point sets, the (approximate) spherical design in this study achieves smaller ratios of  $\|\mathbf{a}_n^{c,t}\|_2$  for degrees  $n = 1, 2, \dots, t$ , demonstrating that the spherical design in this study realizes a more accurate isotropy defined by the 2-norm isotropy indicator (11).

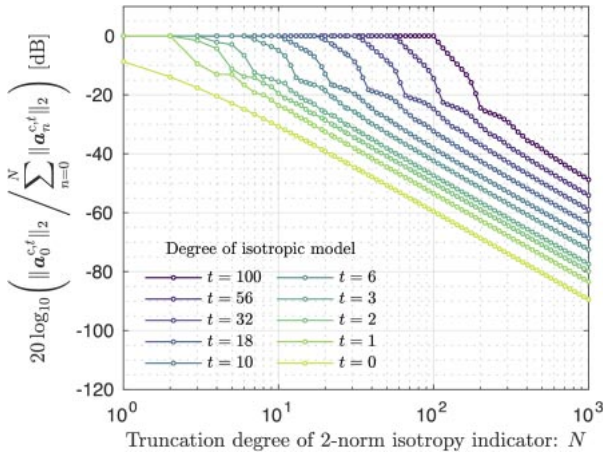
## 5.3. Evaluation of Limited-degree Isotropic Sound Field Model Using 2-norm Isotropy Indicator

Figure 5 shows the numerical value of the 2-norm isotropy indicator (11) for SHECs (27) of select limited-degree isotropic sound field models using approximate spherical designs in this study. 10 degrees  $t$  of isotropic model and 100 truncation degrees  $N$  of the indicator were selected at logarithmically equal intervals from 0 to 100 and from 1 to 1,000, respectively.

The numerical value of the isotropy indicator is 1 (0 dB), indicating a perfect isotropy, when the truncation degree  $N$  of the indicator is less than or equal to the degree



**Fig. 4** Numerical value of measure (25) for isotropic sound field models using (a) MaxDet [24], (b) spherical designs by Chen *et al.* [26], and (c) spherical designs computed in this study. Degrees of isotropic models are  $t = 0, 2, \dots, 100$ . Marker color indicates the degree of the 2-norm  $\|\mathbf{a}_n^{c,t}\|_2$ :  $n = 0, 1, \dots, t$ . Diamonds indicate the ratio of  $\|\mathbf{a}_0^{c,t}\|_2$ , and the dots indicate the ratio of  $\|\mathbf{a}_n^{c,t}\|_2$  for  $n = 1, 2, \dots, t$ .



**Fig. 5** Numerical value of the 2-norm isotropy indicator for select limited-degree isotropic sound field models. The degree  $t$  of isotropic model and truncation degree  $N$  of the 2-norm isotropy indicator were selected at logarithmically equal intervals.

$t$  of the isotropic sound field model. In contrast, the numerical value of the indicator decreases, indicating anisotropy, as the truncation degree of the indicator  $N$  exceeds the degree of the model. (The  $t = 1$  case is the exception because it is likely that the point set converges to the vertices of the regular tetrahedron, which is a spherical 2-design [27], in the optimization.)

It may be confusing that the numerical value of the 2-norm isotropy indicator varies with the truncation degree. However, this nature enables the concept of limited-degree isotropy, which takes advantage of the truncation-degree dependence of the indicator.

## 6. CASE STUDIES

### 6.1. Application of 1-norm Isotropy Indicator to Limited-degree Isotropic Sound Field Model

The 1-norm isotropy indicator was applied to the cumulative DED of the present isotropic sound field model.

Figure 6 shows the numerical value of the 1-norm isotropy indicator (6) applied to the SHECs (27) of select limited-degree isotropic sound field models using approximate spherical designs in this study. Degrees  $t$  of the isotropic models and truncation degrees  $N$  of 1-norm isotropy indicator were selected as described in Sect. 5.3.

The isotropic model for  $t = 0$  is composed of a single plane wave, and therefore, it should be less isotropic than isotropic models of any other degree. Contrary to expectations, the value of the 1-norm isotropy indicator for 0th-degree isotropic model is larger than that for higher-degree isotropic models when greater truncation degree is applied. The single plane wave arrives from the direction of the North Pole, i.e.,  $\theta_{in} = 0$ , in 0th-degree isotropic model. A possible factor of the above result might thus be that, as

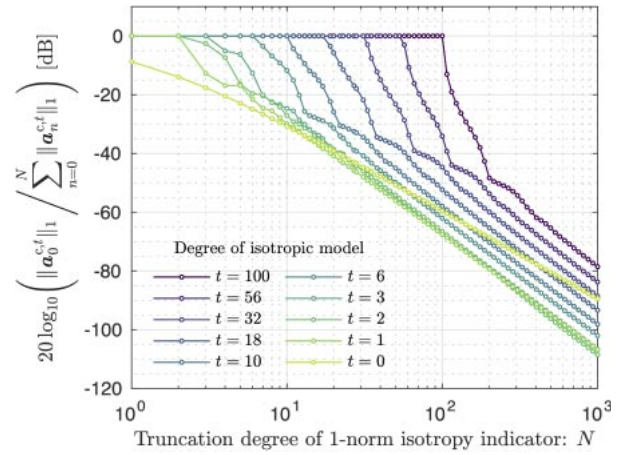


**Fig. 6** The numerical value of the 1-norm isotropy indicator applied to the cumulative DED of the limited-degree isotropic sound field models.

shown in Fig. 2, the 1-norm isotropy indicator tends to overestimate the components arriving from near the direction of the North Pole (the same is true for that of the South Pole, although not shown in the figure). This somewhat troubling results suggest that caution must be applied when evaluating an isotropy using the 1-norm isotropy indicator.

### 6.2. Applications of 2-norm Isotropy Indicator to RIRs

First, the example of an application of the 2-norm isotropy indicator to simulated RIRs is given. As described in details in Ref. [17], geometrical acoustic simulation synthesized the RIRs.

The RIRs were converted to time-frequency domain using short-time Fourier transform, where 256-samples hanning window and 128-samples overlapping were applied. The converted RIRs in the 4,000 Hz octave band were then extracted and converted to spherical-harmonics domain using spherical harmonics up to 4th degree and radial functions [28]. The RIRs in the spherical-harmonics domain were decoded to the amplitudes of plane waves arriving from a spherical 8-design [21]. By Schroeder-integrating the RIRs in the plane-wave domain, a cumulative DED was calculated (see Ref. [9], for example). Finally, the cumulative DED was converted into the spherical-harmonics domain. Note that decay cancellation has not been applied to the RIRs.

Figure 7 shows the numerical value of the 2-norm isotropy indicator (truncation degree  $N = 4$ ) applied to the cumulative DED obtained by the above procedure. Conditions A, D, and E represent absorption conditions in the simulation (see Table 1 and Ref. [17] for graphical visualizations of their DEDs). The lower limit of the vertical axis of the figure is the theoretical minimum of the 2-norm

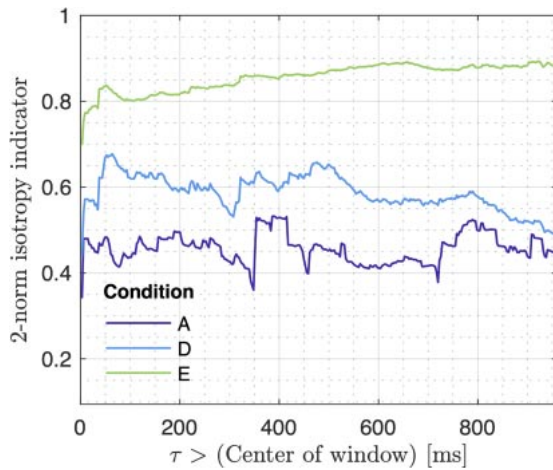


**Fig. 7** The numerical value of the 2-norm isotropy indicator applied to the cumulative DEDs of simulated RIRs.

**Table 1** Absorption coefficient in the simulation of RIR.

Condition	Floor	Ceiling	Walls
A	0.8	0.2	0.2
D	0.2	0.2	0.2
E	0	0	0

isotropy indicator of 4th degree. It is shown that the 2-norm isotropy indicator appropriately reflects the difference in the absorption conditions, suggesting that the 2-norm isotropy indicator can evaluate isotropy of simulated RIRs.

Next, the 2-norm isotropy indicator was applied to measured RIRs (see Ref. [17] for details of measurement).

The RIRs in the 1,000 and 2,000 Hz octave bands were the targets of the evaluation of isotropy. Spherical harmonics up to 2nd degree and spherical 4-design [21] were used for conversion of the RIRs into the domains of spherical harmonics and plane wave, respectively. The other procedures were the same as those described above for the simulated RIRs.

Figure 8 displays the numerical value of the 2-norm isotropy indicator (truncation degree  $N = 2$ ) applied to the cumulative DED of the measured RIRs. The lower limit of the vertical axis of the figure is the theoretical minimum of the 2-norm isotropy indicator of 2nd degree.

For both 1,000 and 2,000 Hz octave bands, values of the 2-norm isotropy indicator decrease rapidly when direct sound arrives ( $t = 0$  ms). Sensitivity of the 2-norm isotropy indicator is similar to that of a comparable isotropy indicator [9]. However, the value of the indicator tends to be larger than that for the simulated RIRs (Fig. 7). One possible implication of this is that the 2-norm isotropy indicator suffers from electrical noise generated by transducers. Further research is required to establish the validity

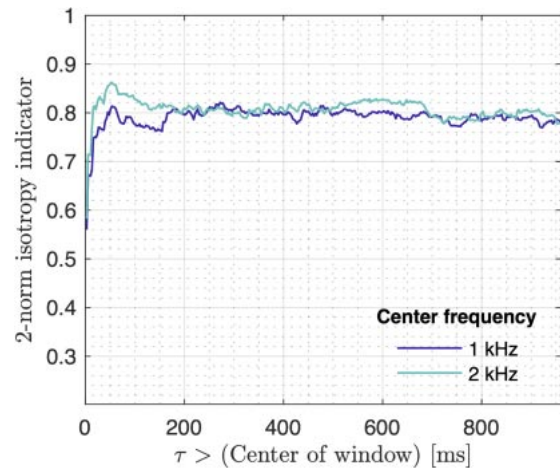


**Fig. 8** The numerical value of the 2-norm isotropy indicator applied to the cumulative DEDs of measured RIRs.

of the 2-norm isotropy indicator applied to measured signals.

## 7. CONCLUSIONS

The 2-norm isotropy indicator was presented by modifying the existing isotropy indicator from the viewpoint of rotational invariance. The numerical and experimental investigations of the 2-norm isotropy indicator have shown its usefulness (sufficiently high sensitivity) and limitations (possible vulnerability to noise).

Using the 2-norm isotropy indicator, this paper conceptualized (i) an ideal isotropy for a given limitation on the directional resolution and (ii) an isotropic sound field composed of a finite number of plane waves arriving from directions sampled with the spherical design. It is theoretically shown that a finite number of plane waves can synthesize a perfectly isotropic sound field by limiting the maximum degree of the isotropy.

The present results might contribute to a better understanding of the isotropy of a sound field.

## ACKNOWLEDGEMENTS

This study was partly supported by a Research Fellowship for Young Scientists (22J20416) and Grants-in-Aid for Scientific Research (JP19H04153 and JP19H04145) from JSPS, Japan. The authors thank Prof. Toshiki Hanyu (Nihon University Junior College, Japan) for the valuable discussions. The authors are also grateful to Prof. Takao Tsuchiya (Doshisha University, Japan) and Mr. Hiraku Okumura (Yamaha Co., Japan) for their support in the measurement of RIRs.

## REFERENCES

- [1] ISO 354:2003, "Acoustics — Measurement of sound absorption in a reverberation room" (International Organization for

- Standardization, Geneva, Switzerland, 2003).
- [2] L. L. Beranek, *Concert & Opera Halls: How They Sound* (Acoustical Society of America, Woodbury, NY, 1996).
- [3] J. S. Bradley and G. A. Soulodre, “The influence of late arriving energy on spatial impression,” *J. Acoust. Soc. Am.*, **97**, 2263–2271 (1995).
- [4] M. Morimoto, K. Nakagawa and K. Iida, “The relation between spatial impression and the law of the first wavefront,” *Appl. Acoust.*, **69**, 132–140 (2008).
- [5] T. Okano, L. L. Beranek and T. Hidaka, “Relations among interaural cross-correlation coefficient (IACCE), lateral fraction (LFE), and apparent source width (ASW) in concert halls,” *J. Acoust. Soc. Am.*, **104**, 255–265 (1998).
- [6] W. C. Sabine, *Collected Papers on Acoustics* (Harvard University Press, Cambridge, MA, 1922).
- [7] M. Nolan, E. F.-Grande, J. Brunskog and C. H. Jeong, “A wavenumber approach to quantifying the isotropy of the sound field in reverberant spaces,” *J. Acoust. Soc. Am.*, **143**, 2514–2526 (2018).
- [8] G. D. Galdo, M. Taseska, O. Thiergart, J. Ahonen and V. Pulkki, “The diffuse sound field in energetic analysis,” *J. Acoust. Soc. Am.*, **131**, 2141–2151 (2012).
- [9] M. Berzborn and M. Vorländer, “Directional sound field decay analysis in performance spaces,” *Build. Acoust.*, **28**, 249–263 (2021).
- [10] B. N. Gover, J. G. Ryan and M. R. Stinson, “Microphone array measurement system for analysis of directional and spatial variations of sound fields,” *J. Acoust. Soc. Am.*, **112**, 1980–1991 (2002).
- [11] B. N. Gover, J. G. Ryan and M. R. Stinson, “Measurements of directional properties of reverberant sound fields in rooms using a spherical microphone array,” *J. Acoust. Soc. Am.*, **116**, 2138–2148 (2004).
- [12] E. Meyer and R. Thiele, “Raumakustische Untersuchungen in zahlreichen Konzertsälen und Rundfunkstudios unter Antoendung neuerer Meßverfahren,” *Acta Acust. united Ac.*, **6**, 425–444 (1956).
- [13] M. Nolan, M. Berzborn and E. F.-Grande, “Isotropy in decaying reverberant sound fields,” *J. Acoust. Soc. Am.*, **148**, 1077–1088 (2020).
- [14] K. J. Ebeling, “Statistical properties of random wave fields,” in *Physical Acoustics*, W. P. Mason and R. N. Thurston, Eds., Vol. XVII (Academic Press, Orland, Fla., 1984), pp. 233–310.
- [15] M. Nolan, E. F.-Grande, J. Brunskog, A. Richard and C. H. Jeong, “A wavenumber approach to characterizing the diffuse field conditions in reverberation rooms,” *Proc. 22nd Int. Congr. Acoust.*, Paper ICA2016-578, Buenos Aires (2016).
- [16] Q. T. L. Gia, I. H. Sloan, R. S. Womersley and Y. G. Wang, “Isotropic sparse regularization for spherical harmonic representations of random fields on the sphere,” *Appl. Comput. Harmon. Anal.*, **49**, 257–278 (2020).
- [17] Y. Izumi and M. Otani, “Relation between Direction-of-Arrival distribution of reflected sounds in late reverberation and room characteristics: Geometrical acoustics investigation,” *Appl. Acoust.*, **176**, 107805 (2021).
- [18] A. David and S. J. Elliott, “Numerical studies of actively generated quiet zones,” *Appl. Acoust.*, **41**, 63–79 (1994).
- [19] J. J. G.-Bonito and S. J. Elliott, “Local active control of diffracted diffuse sound fields,” *J. Acoust. Soc. Am.*, **98**, 1017–1024 (1995).
- [20] Ph. Delsarte, J.-M. Goethals and J. J. Seidel, “Spherical codes and designs,” *Geom. Dedicata*, **6**, 363–388 (1977).
- [21] R. S. Womersley, “Efficient spherical designs with good geometric properties,” in *Contemporary Computational Mathematics—A Celebration of the 80th Birthday of Ian Sloan* (Springer International, Cham, 2018), pp. 1243–1285.
- [22] K. Levenberg, “A method for the solution of certain non-linear problems in least squares,” *Q. Appl. Math.*, **2**, 164–168 (1944).
- [23] D. W. Marquardt, “An algorithm for least-squares estimation of nonlinear parameters,” *J. Soc. Ind. Appl. Math.*, **11**, 431–441 (1963).
- [24] I. H. Sloan and R. S. Womersley, “Extremal systems of points and numerical integration on the sphere,” *Adv. Comput. Math.*, **21**, 107–125 (2004).
- [25] MATLAB, *Version 9.11.0 (R2021b)* (The MathWorks, Inc., Natick, MA, 2021).
- [26] X. Chen, A. Frommer and B. Lang, “Computational existence proofs for spherical t-designs,” *Numer. Math.*, **117**, 289–305 (2011).
- [27] R. H. Hardin and N. J. A. Sloane, “McLaren’s improved snub cube and other new spherical designs in three dimensions,” *Discrete Comput. Geom.*, **15**, 429–441 (1996).
- [28] B. Rafaely, *Fundamentals of Spherical Array Processing* (Springer Nature Switzerland, Cham, 2019).
- [29] W. Freeden and M. Gutting, *Special Functions of Mathematical (Geo-)physics* (Springer Basel, Basel, 2013).

## APPENDIX A: SPHERICAL HARMONICS

### A.1. Definitions of complex- and real-valued spherical harmonics

For  $n = 0, 1, 2, \dots$ , and  $m = 0, \pm 1, \dots, \pm n$ , complex-valued spherical harmonics [29, Ex. 4.3.32] and real-valued spherical harmonics [29, Ex. 4.3.33] are defined as

$$Y_{n,m}^{\mathbb{C}}(\theta, \phi) := (-1)^m \cdot L_{n,m}(\cos \theta) \cdot \frac{e^{im\phi}}{\sqrt{2\pi}}, \quad (\text{A.1})$$

$$Y_{n,m}^{\mathbb{R}}(\theta, \phi) := L_{n,|m|}(\cos \theta) \cdot \begin{cases} \frac{\cos(m\phi)}{\sqrt{\pi}}, & m < 0, \\ 1, & m = 0, \\ \frac{\sin(m\phi)}{\sqrt{\pi}}, & m > 0, \end{cases} \quad (\text{A.2})$$

where  $e$  is the Napier number and  $L_{n,m}$  is fully normalized associated Legendre polynomials [25, legendre( $n$ ,  $\cos(\theta)$ , ‘norm’)]. Here,  $n$  and  $m$  are the degree and order of the spherical harmonics, respectively, and  $0 \leq \theta \leq \pi$  and  $-\pi \leq \phi < \pi$  are the angular coordinates in the spherical coordinate system.

### A.2. Relational formula between complex- and real-valued spherical harmonics

For  $n = 0, 1, 2, \dots$ , the following relational formula holds between complex- and real-valued spherical harmonics

$$Y_{n,m}^{\mathbb{C}}(\theta, \phi) = \begin{cases} \frac{Y_{n,m}^{\mathbb{R}}(\theta, \phi) - iY_{n,-m}^{\mathbb{R}}(\theta, \phi)}{\sqrt{2}}, & m < 0. \\ Y_{n,m}^{\mathbb{R}}(\theta, \phi), & m = 0. \\ \frac{Y_{n,-m}^{\mathbb{R}}(\theta, \phi) + iY_{n,m}^{\mathbb{R}}(\theta, \phi)}{(-1)^m \cdot \sqrt{2}}, & m > 0. \end{cases} \quad (\text{A.3})$$

**Derivation of the relational formula**

**$m = 0$  case**

From definitions (A.1) and (A.2),  $Y_{n,m}^{\mathbb{C}}(\theta, \phi) = Y_{n,m}^{\mathbb{R}}(\theta, \phi)$  clearly holds.

**$m < 0$  case**

From the following order-reflection formula of a fully normalized associated Legendre polynomial, which is given as

$$L_{n,-m}(z) = (-1)^m \cdot L_{n,m}(z), \quad (\text{A.4})$$

the following equation holds

$$L_{n,|\pm m|}(z) = L_{n,-m}(z) = (-1)^m \cdot L_{n,m}(z) \quad (\text{A.5})$$

for  $m = -1, -2, \dots, -n$ . Equation (A.5) and Euler's formula lead to the following relational formula

$$\begin{aligned} Y_{n,m}^{\mathbb{R}}(\theta, \phi) &= L_{n,|m|}(\cos \theta) \cdot \frac{\cos(m\phi)}{\sqrt{\pi}} \\ &= (-1)^m \cdot L_{n,m}(\cos \theta) \cdot \frac{\cos(m\phi)}{\sqrt{\pi}} \\ &= \sqrt{2} \cdot \text{Re}[Y_{n,m}^{\mathbb{C}}(\theta, \phi)], \quad -1 \leq m \leq -n, \end{aligned} \quad (\text{A.6})$$

where  $\text{Re}[\cdot]$  is the real part of the complex number.

In contrast, considering the order-reflected real-valued spherical harmonics, the following relation can be derived

$$\begin{aligned} Y_{n,-m}^{\mathbb{R}}(\theta, \phi) &= L_{n,|-m|}(\cos \theta) \cdot \frac{\sin(-m\phi)}{\sqrt{\pi}} \\ &= (-1)^m \cdot L_{n,m}(\cos \theta) \cdot \frac{-\sin(m\phi)}{\sqrt{\pi}} \\ &= -\sqrt{2} \cdot \text{Im}[Y_{n,m}^{\mathbb{C}}(\theta, \phi)], \quad -1 \leq m \leq -n, \end{aligned} \quad (\text{A.7})$$

where  $\text{Im}[\cdot]$  is the imaginary part of the complex number.

From Eqs. (A.6) and (A.7), the following formula can be derived

$$Y_{n,m}^{\mathbb{C}}(\theta, \phi) = \frac{Y_{n,m}^{\mathbb{R}}(\theta, \phi) - iY_{n,-m}^{\mathbb{R}}(\theta, \phi)}{\sqrt{2}}, \quad (\text{A.8})$$

for  $m = -1, -2, \dots, -n$ .

**$m > 0$  case**

Using the order-reflection formula of complex-valued spherical harmonics

$$Y_{n,-m}^{\mathbb{C}}(\theta, \phi) = (-1)^m \cdot \overline{Y_{n,m}^{\mathbb{C}}(\theta, \phi)}, \quad m = 0, \pm 1, \dots, \pm n, \quad (\text{A.9})$$

and Eq. (A.8), the following relation can be derived

$$\begin{aligned} Y_{n,-m}^{\mathbb{C}}(\theta, \phi) &= (-1)^m \cdot \overline{Y_{n,m}^{\mathbb{C}}(\theta, \phi)} \\ &= (-1)^m \cdot \frac{\overline{Y_{n,m}^{\mathbb{R}}(\theta, \phi) - iY_{n,-m}^{\mathbb{R}}(\theta, \phi)}}{\sqrt{2}} \\ &= (-1)^m \cdot \frac{Y_{n,m}^{\mathbb{R}}(\theta, \phi) + iY_{n,-m}^{\mathbb{R}}(\theta, \phi)}{\sqrt{2}} \end{aligned} \quad (\text{A.10})$$

for  $-m = 1, 2, \dots, n$ . Rewriting the above equation using  $m$  instead of  $-m$  yields

$$\begin{aligned} Y_{n,m}^{\mathbb{C}} &= (-1)^{-m} \cdot \frac{Y_{n,-m}^{\mathbb{R}}(\theta, \phi) + iY_{n,m}^{\mathbb{R}}(\theta, \phi)}{\sqrt{2}} \\ &= \frac{Y_{n,-m}^{\mathbb{R}}(\theta, \phi) + iY_{n,m}^{\mathbb{R}}(\theta, \phi)}{(-1)^m \cdot \sqrt{2}}, \quad m = 1, 2, \dots, n. \end{aligned} \quad (\text{A.11})$$

The derivation of relational formula (A.3) is complete.  $\square$

**APPENDIX B: PROOF OF PROPOSITION 1**

The Proposition is restated here for convenience.

**Proposition.**  $\hat{\Phi}_Q = \{(\hat{\theta}_q, \hat{\phi}_q); q = 1, 2, \dots, Q\}$  is a point set on the unit sphere  $\mathbb{S}^2$ . For  $n = 1, 2, \dots, t$  and  $m = 0, \pm 1, \dots, \pm n$ , the following two equations are equivalent

$$\sum_{q=1}^Q Y_{n,m}^{\mathbb{R}}(\hat{\theta}_q, \hat{\phi}_q) = 0. \quad (\text{a})$$

$$\sum_{q=1}^Q Y_{n,m}^{\mathbb{C}}(\hat{\theta}_q, \hat{\phi}_q) = 0. \quad (\text{b})$$

**Proof**

**$m = 0$  case**

From relational formula (A.3),  $Y_{n,m}^{\mathbb{C}}(\theta, \phi) = Y_{n,m}^{\mathbb{R}}(\theta, \phi)$  holds. Thus, (a)  $\Leftrightarrow$  (b) clearly holds.

**Proof of (a)  $\Rightarrow$  (b)**

**$m < 0$  case**

Using the relational formula (A.3) for  $m < 0$ , the following holds

$$\begin{aligned} \sum_{q=1}^Q Y_{n,m}^{\mathbb{C}}(\hat{\theta}_q, \hat{\phi}_q) &= \sum_{q=1}^Q \frac{Y_{n,m}^{\mathbb{R}}(\hat{\theta}_q, \hat{\phi}_q) - iY_{n,-m}^{\mathbb{R}}(\hat{\theta}_q, \hat{\phi}_q)}{\sqrt{2}} \\ &= \frac{1}{\sqrt{2}} \sum_{q=1}^Q Y_{n,m}^{\mathbb{R}}(\hat{\theta}_q, \hat{\phi}_q) \\ &\quad - \frac{i}{\sqrt{2}} \sum_{q=1}^Q Y_{n,-m}^{\mathbb{R}}(\hat{\theta}_q, \hat{\phi}_q) \\ &= 0. \end{aligned}$$

**$m > 0$  case**

Similarly, using relational formula (A.3) for  $m > 0$ , the following holds

$$\sum_{q=1}^Q Y_{n,m}^C(\hat{\theta}_q, \hat{\phi}_q) = \sum_{q=1}^Q \frac{Y_{n,-m}^R(\hat{\theta}_q, \hat{\phi}_q) + iY_{n,m}^R(\hat{\theta}_q, \hat{\phi}_q)}{(-1)^m \cdot \sqrt{2}} \quad \sum_{q=1}^Q \operatorname{Re}[Y_{n,m}^C(\hat{\theta}_q, \hat{\phi}_q)] = 0. \quad (\text{B}\cdot 1)$$

$$= \frac{1}{(-1)^m \cdot \sqrt{2}} \sum_{q=1}^Q Y_{n,-m}^R(\hat{\theta}_q, \hat{\phi}_q) \quad \sum_{q=1}^Q \operatorname{Im}[Y_{n,m}^C(\hat{\theta}_q, \hat{\phi}_q)] = 0. \quad (\text{B}\cdot 2)$$

$$+ \frac{i}{(-1)^m \cdot \sqrt{2}} \sum_{q=1}^Q Y_{n,m}^R(\hat{\theta}_q, \hat{\phi}_q)$$

= 0.

$m < 0$  case

Using Eq. (B-1) and relational formula (A-3) for  $m < 0$ , the following holds

$$\square \quad \sum_{q=1}^Q Y_{n,m}^R(\hat{\theta}_q, \hat{\phi}_q) = \sqrt{2} \cdot \sum_{q=1}^Q \operatorname{Re}[Y_{n,m}^C(\hat{\theta}_q, \hat{\phi}_q)] = 0.$$

$m > 0$  case

Using Eq. (B-2) and relational formula (A-3) for  $m > 0$ , the following holds

$$\sum_{q=1}^Q Y_{n,m}^R(\hat{\theta}_q, \hat{\phi}_q) = (-1)^m \cdot \sqrt{2} \cdot \sum_{q=1}^Q \operatorname{Im}[Y_{n,m}^C(\hat{\theta}_q, \hat{\phi}_q)] = 0.$$

□

Thus, Proposition 1 is proven. □

**Proof of (a) ⇐ (b)**

Equation (b) can be divided into the real and imaginary parts and is given as

$$\begin{aligned} 0 &= \sum_{q=1}^Q Y_{n,m}^C(\hat{\theta}_q, \hat{\phi}_q) \\ &= \sum_{q=1}^Q \operatorname{Re}[Y_{n,m}^C(\hat{\theta}_q, \hat{\phi}_q)] + i \sum_{q=1}^Q \operatorname{Im}[Y_{n,m}^C(\hat{\theta}_q, \hat{\phi}_q)]. \end{aligned}$$

Hence, the following two equations hold